Millimeter-wave 45º linearly polarized corporate-fed slot array antenna with low profile and reduced complexity

You, Yang; Lu, Yunlong; Skaik, Talal; Wang, Yi; Huang, Jifu

DOI:
10.1109/TAP.2021.3069561

Millimeter-Wave 45° Linearly Polarized Corporate-Fed Slot Array Antenna With Low Profile and Reduced Complexity

Yang You, Yunlong Lu, Talal Skaik, Yi Wang, and Jifu Huang

***Abstract*—A millimeter-wave 45° linearly polarized corporate-fed slot array antenna is presented in this communication. A key feature is the much reduced number of metallic layers and therefore the complexity of the array, as compared with other competitive designs. With the reduced antenna profile, high cross polarization discrimination (XPD) and low sidelobe level (SLL) are still achieved by a combination of techniques. The back cavity of the 2×2-slot sub-array is optimized to confine the H-field along the direction of the radiation slots, enhancing its XPD. Stubs are loaded in the same cavity to compensate for the phase imbalance, suppressing both cross-polarization and grating lobes without introducing additional metallic layers. Combining these features, the proposed array antenna demonstrates high performance with only three essential metallic layers. A prototype with 8×8 radiation slots at Ka-band is implemented for demonstration. Experimental results show that the grating lobes are suppressed to below -30.5 dB, and the first SLL (FSLL) of less than -26.2 dB. XPD of more than 31.3 dB is achieved over the frequency range of 26.5 GHz - 32 GHz. The peak gain of better than 25 dBi and antenna efficiency of over 71.7% are also obtained over the same frequency range.**

***Index Terms*—Slot Array antenna, millimeter wave antennas, high efficiency, low sidelobe, high cross polarization discrimination.**

I. Introduction

With the explosive growth in data communication, utilizing millimeter-wave (mmW) bands to improve the system overall performance becomes a promising solution for the fifth-generation (5G) mobile communications [1], [2]. Different from most of the current communication system with operating frequency below 6 GHz, mmW bands offer wider operating bandwidth, smaller circuits and antenna sizes [3]-[5]. The World Radio-Communication Conference (WRC) has recommended the mmW bands of 24 GHz and beyond as the frequency band for 5G mmW communications. The Ka-band is one of the most favorable bands [6], [7]. In order to achieve high-speed and stable communication over a long distance in 5G mmW scenario, the antenna should have high gain, high efficiency, low sidelobe level (SLL) and high cross polarization discrimination (XPD) [8]-[10].

Microstrip structure is a common choice for various types of antennas. But the relatively large dielectric loss and unwanted parasitic radiation decreases the antenna efficiency, especially in mmW high-gain arrays [11]-[13]. In contrast, waveguide has lower loss and is a better transmission structure for mmW antennas.

This work was supported partly by National Key R&D Program of China under Project 2018YFB1802100, in part by National Natural Science Foundation of China under Projects 61801252, U1809203, and 61631012, in part by Zhejiang Natural Science Foundation under Project LY21F010002 and K.C. Wong Magna Fund in Ningbo University. Yi Wang was supported by the U.K. Engineering and Physical Science Research Council under Contract EP/S013113/1. (Corresponding author: *Yunlong Lu*)

Y. You, Y. Lu, and J. Huang are with the Faculty of Electrical Engineering and Computer Science, Ningbo University, Ningbo, Zhejiang, 315211, China (e-mail: luyunlong@nbu.edu.cn).

T. Skaik and Y. Wang is with School of Engineering, University of Birmingham, B15 2TT, United Kingdom (e-mail: y.wang.1@bham.ac.uk).

Color versions of one or more of the figures in this communication are available online at http://ieeexplore.ieee.org.

Digital Object Identifier 10.1109/TAP.2016.xxx

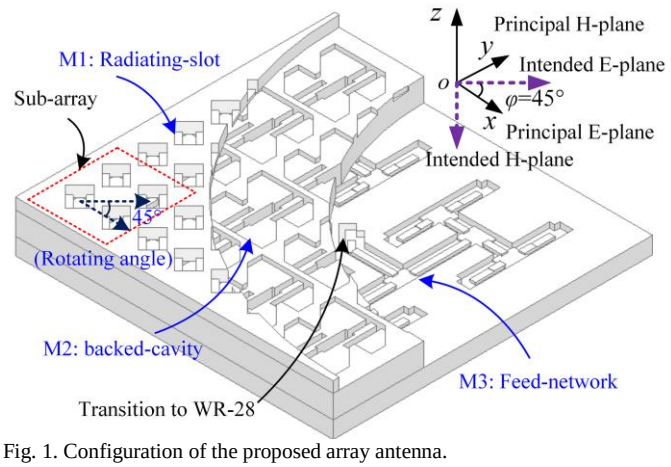

Fig. 1. Configuration of the proposed array antenna.

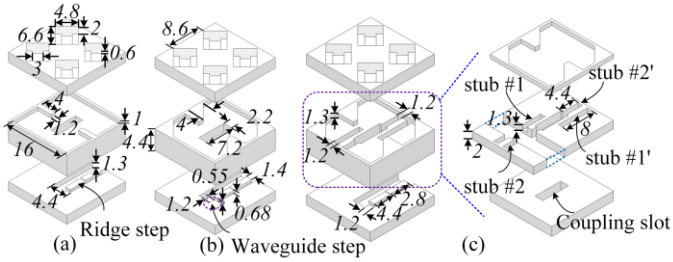

Fig. 2. Evolution of sub-array design. (a) Starting design (Type I); (b) Sub-array with XPD enhancement (Type II); (c) Sub-array with XPD enhancement and grating lobe suppression (Type III). All dimensions are given in millimeters.

Substrate integrated waveguide (SIW) and air-filled hollow waveguide are the two main categories of waveguide structures. A lot of antennas based on SIW have been reported. However, the existence of dielectric loss inevitably affects the antenna efficiency [14], [15]. Slot array antennas based on air-filled waveguide provide optimal antenna efficiency and has been widely used in high-performance antenna systems [16], [17].

Low SLL is a key characteristic of antennas, as it means reduced interference and improved system performance. Applying amplitude tapering to the array elements is a major technique to realize low SLLs [18]-[20]. However, this normally requires complicated power dividers with different power ratios in the feed network. It not only increases the complexity of the feed network, but also decreases the antenna efficiency. An alternative way to achieve low SLLs without sacrificing antenna efficiency is to use 45° linearly polarized antennas [21]-[26]. It shifts the polarization to the diagonal plane of the uniformly excited square array where sidelobes are suppressed. Two main methods have been reported for the design of a 45° linearly polarized antenna. One uses a separate 45° linear polarizer loaded on top of the uniformly excited array antenna [22]. This extra polarizer increases the antenna profile and introduces additional insertion loss. Moreover, the installation of this separate polarizer requires a fixture, which complicates the antenna structure.

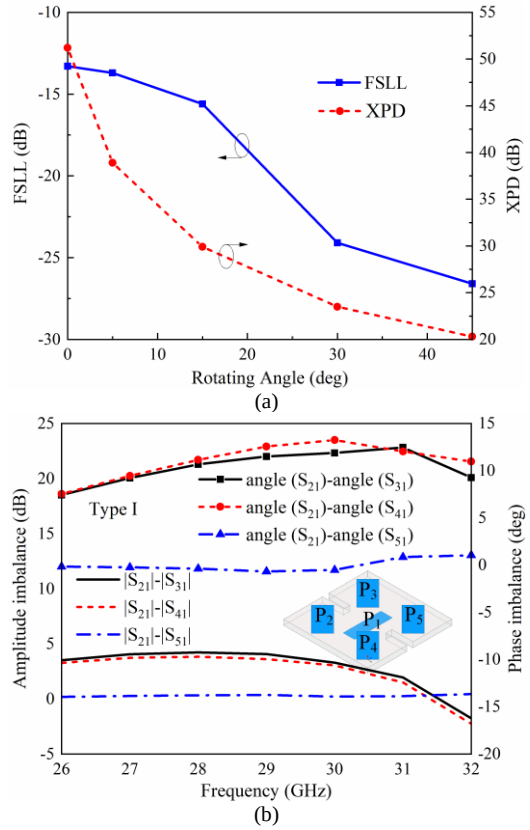

Fig. 3. (a) Simulated XPD and FSLL of an array antenna based on Type I in the intended E-plane; (b) Simulated amplitude and phase imbalance in cavity-backed of Type I.

Another technique is to directly rotate the radiation slots to the desired non-principal plane [14], [23], [24]. No additional polarizer is required. A slot sub-array excited by a vertical power divider was usually used as the basic sub-array. In order to improve the antenna efficiency and operation bandwidth, the radiation slots in the sub-array should be wide. However, this would cause increased SLLs due to the appearance of grating lobes, as a result of the amplitude and phase imbalances among the rotated slots. The cross-polarization patterns also suffer as the rotation angle of the radiation slots increases. The solutions reported in [23] and [24] were: (i) To mitigate the grating lobes, an additional layer of exciting slot was inserted and optimized between the cavity-backed power divider and radiation slots; (ii) For XPD enhancement, the height of the radiation slots was increased or another layer of narrow-slot pairs added to the top of the radiation slots. With the benefits of diffusion bonding technique used in [23] and [24], electromagnetic leakage from these additional metallic layers is less of a problem [25]. However, these additional circuit layers will add significant complexity and leakage paths to antennas manufactured using other fabrication processes which require multi-layer assembly by tightening screws. In [26], a 10°-tilted radiation slots were utilized to realize the low SLLs without any extra layers or thickening the radiation slots. Unfortunately, the XPD in [26] suffered when a larger titling angle was used to further improve the SLLs. It is a significant design challenge to improve XPD and SLLs without increasing the layers of the antenna.

This communication presents an mmW high-performance 45° linearly polarized array antenna with only three essential metallic layers: the radiation slot layer, the cavity-backed layer and the feed network layer. Without any additional metallic layers, the cross-polarization patterns and grating lobes are suppressed by only optimizing the back-cavity layer. The proposed array antenna exhibits low SLLs, high XPD and high antenna efficiency. The paper is organized as follows: Section II describes the antenna analysis and design. Section III presents the experimental validation, followed by conclusion in Section IV.

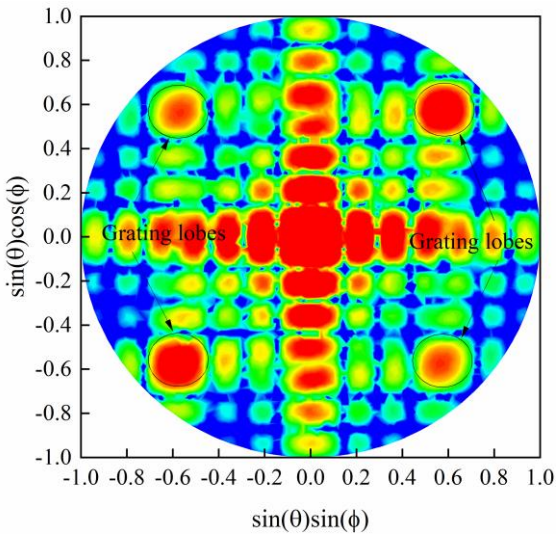

Fig. 4. Simulated 3-D radiation pattern of 4×4 sub-arrays based on Type I at the center frequency.

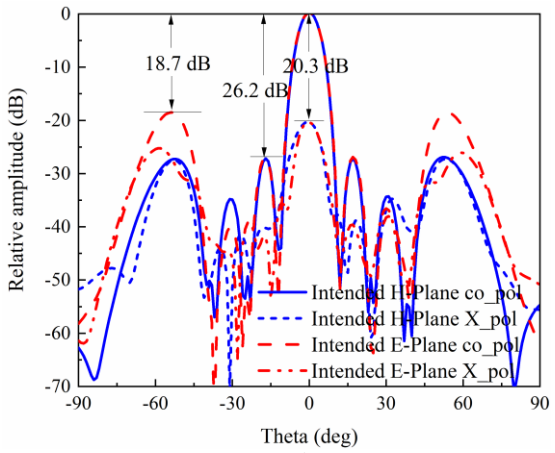

Fig. 5. Simulated 2-D radiation patterns of 4×4 sub-arrays based on Type I at the center frequency.

II. Antenna Design and Analysis

A. Antenna Configuration

Fig. 1 shows the configuration of the 8×8 45° linearly polarized slot array antenna. It consists of three metallic layers: radiation-slot layer (M1), cavity-backed layer (M2), and feed-network layer (M3). A combination of 16 (4×4) 1-to-4 vertical power dividers in M2 and 1-to-16 planar power divider in M3 is used to excite the 8×8 radiation slots in M1. A 2×2-slot sub-array is adopted as the building block element. Different from [23] and [24], the radiation slots here are directly rotated by 45° with no additional circuit layer is used. Compared with [23], the proposed antenna is significantly simplified and the number of metallic layers is reduced. The coordinate system utilized in this design is indicated in Fig. 1. The principal E- (φ = 0°) and H- (φ = 90°) planes and the intended E- (φ = 45°) and H- (φ = 135°) planes are also defined in Fig. 1. The concerned frequency band is 26.5–32 GHz, and the design details are given as follows. All the simulations are carried out in Ansoft HFSS.

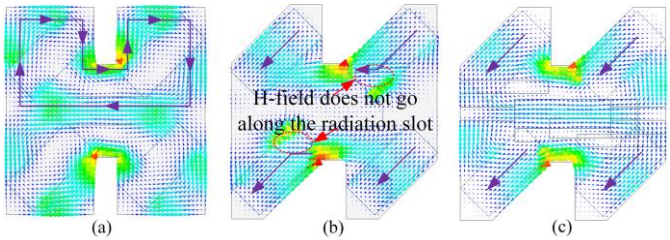

Fig. 6. Simulated H-field distributions in the backed cavities of (a) Type I, (b) Type II and (c) Type III.

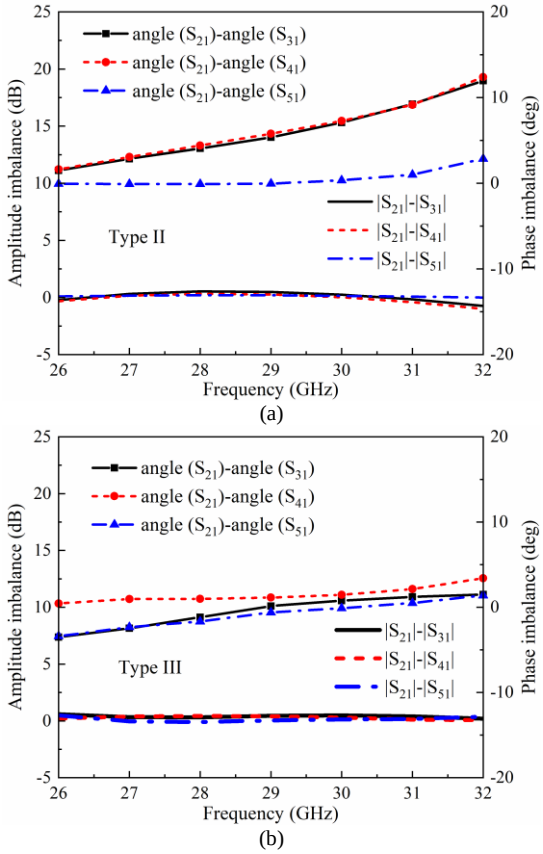

Fig. 7. Simulated amplitude and phase imbalances in the backed cavities of (a) Type II and (b) Type III.

B. Sub-array Analysis and Array Antenna Synthesis

The design evolution of the sub-array is shown in Fig. 2. All the sub-arrays have the same radiation slots and feed structure. It starts with the sub-array (Type I) in Fig. 2(a). The design details can be found in [23], [24], [26] and [27]. The 45°-tilted, stepped and flared radiation slots are used to suppress external mutual coupling between slots and improve the impedance bandwidth, while maintaining good first sidelobe level (FSLL) characteristics [27]. The space between adjacent radiation slots is chosen to avoid the grating lobes. It is 8.6 mm in this work (about $0.9\lambda_{min}$, λ_{min} is the free space wavelength at 32 GHz). The ridge and waveguide steps are utilized to achieve the wideband transition from output single-ridge waveguide structures of the feed network to hollow-waveguide based coupling slots. Other optimized parameters are shown in Fig. 2 (a). As analyzed in [21], the FSLL decreases with the rotation angle of the radiation slot. However, this will deteriorate XPD if no mitigation is made. Fig. 3(a) shows the simulated XPD and FSLL with different rotation angles at the center frequency of 29 GHz in the intended E-plane. These results are obtained by simulating an array consisting of 4×4 Type I sub-arrays. Other results of the 4×4 sub-arrays in the following text are obtained by the same method. At 45°, the FSLL is lower than -26 dB whereas the XPD is only about 20 dB. Due to the asymmetry introduced by the 45° slots, the amplitude and phase distributions between the adjacent radiation slots become unbalanced. Fig. 3(b) shows the amplitude and phase responses in the cavity-backed design of Type I. Although the excitation signals between the two output ports along the diagonal plane (e.g. ports P2 and P5, ports P3 and P4) are approximately equal, an amplitude variation of -3.2 dB to +3.8 dB and a phase imbalance of 6° to 13.6° over the frequency band of 26-32 GHz can be observed between ports P2 (P4) and P3 (P5). These imbalances lead to rising grating lobes. Fig. 4 shows the 3-D radiation pattern of a 4×4-sub-array antenna based on Type I at 29 GHz. Four grating lobes appear in the diagonal planes of φ = 45° and 135°. For further clarity, the 2-D radiation patterns in the intended E- and H-planes are plotted in Fig. 5. The grating lobe level (GLL), in the region of $\theta \in$ [-70°, -45°] and [45°, 70°], is about -18.7 dB and higher than the FSLL (about -26.2 dB).

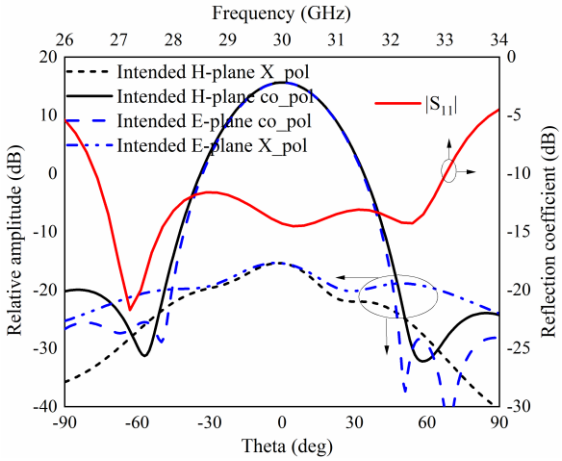

Fig. 8. Simulated reflection coefficient and radiation patterns of the Type III design.

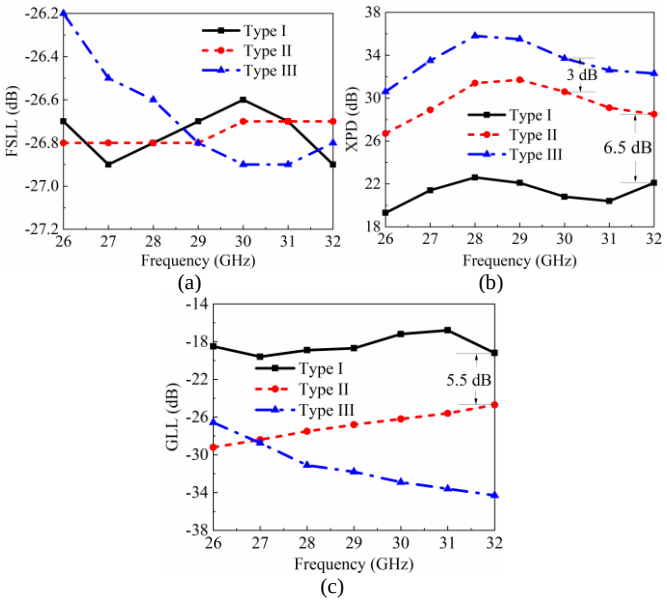

Fig. 9. Simulated 4×4-sub-array antenna performances. (a) FSLL, (b) XPD and (c) GLL in the intended E-plane.

A key objective of this work is to suppress the cross-polarization patterns and grating lobes without introducing additional metallic layers. First of all, four triangular blocks are added to the cavity. This becomes the Type II sub-array shown in Fig. 2(b). The dimensions of triangular blocks are optimized to confine the H-field in the back cavity mainly along the length of radiation slots (the

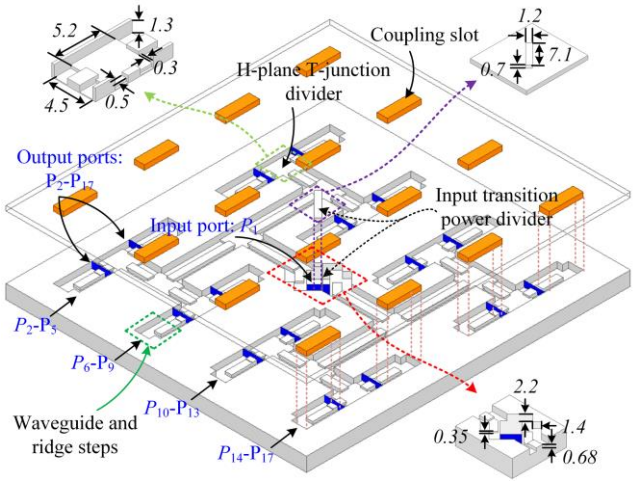

Fig. 10. Configuration of the feed network. For clarity, the "coupling slots" are shown in orange. All dimensions are given in millimeters.

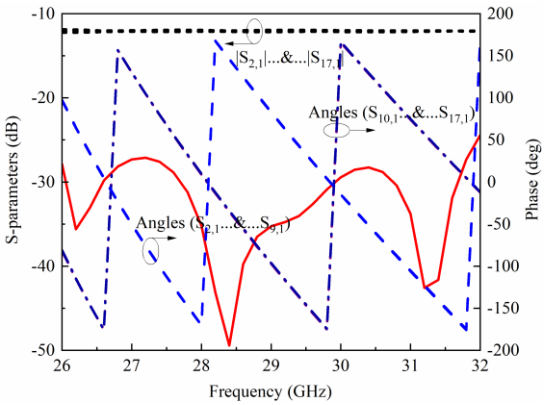

Fig. 11. Simulated S-parameters of the feed network.

intended H-plane direction), which helps to improve the XPD. This is shown in Fig. 6, comparing the cases with and without the triangular blocks. The amplitude imbalance in the cavity-backed design of Type II is also improved, as shown in Fig. 7(a). The variation is reduced to ±0.6 dB. However, the phase imbalance is still prominent (1.5° - 12.4° within the frequency range of 26 - 32 GHz). This phase imbalance causes a residual H-field that does not follow the direction of the radiation slot, as marked out in Fig. 6(b).

In order to compensate for the phase imbalance, two stubs (#1 and #1' as shown in Fig. 2) are added to the back cavity. Two further stubs #2 and #2' are introduced to improve input impedance matching in the 1-to-4 vertical power divider. The sub-array after these modifications is denoted Type III, as shown in Fig. 2(c). The H-field distribution in Type III is shown in Fig. 6(c). Compared with the Type II sub-array, it is further confined along the length of radiation slots. Fig. 7(b) shows the amplitude and phase responses. The amplitude variation is within ±0.2 dB and the phase variation is reduced to within ±2°. Fig. 8 shows the reflection coefficient and radiation patterns of the Type-III. The reflection coefficient is lower than -10 dB over the frequency range of 26.5 - 33 GHz, and the SLL and XPD are better than -35 dB and 31 dB at 29 GHz.

The simulated performances of an array with 4×4 sub-arrays based on Types I, II and III are shown in Fig. 9. It can be seen that the modification in the back cavity does not affect much of the FSLLs, which is maintained below -26 dB. Compared with the Type-I array, the XPD and GLL based on Type II are improved by more than 6.5 dB and 5.5 dB over the operating band of 26.5-32 GHz, as shown in Fig. 9 (b) and (c). This is achieved by the optimized H-field distribution in the back cavity, which balances the output amplitude distributions of the 1-to-4 vertical power divider, as shown in Fig.

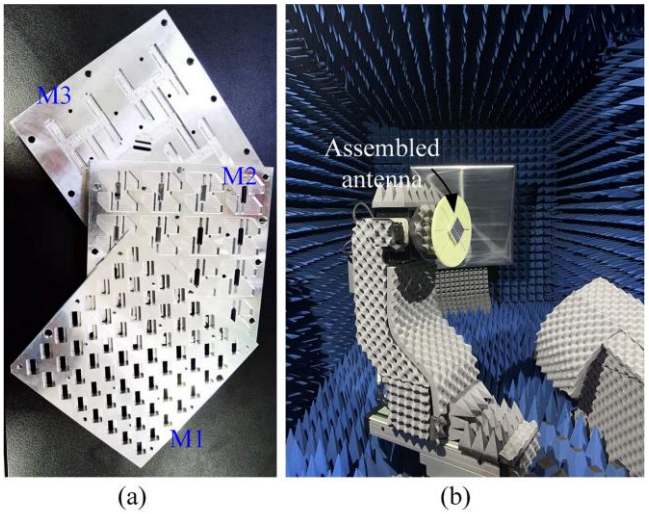

Fig. 12. Photographs of the fabricated prototype. (a) Separated blocks, (b) assembled antenna and test environment.

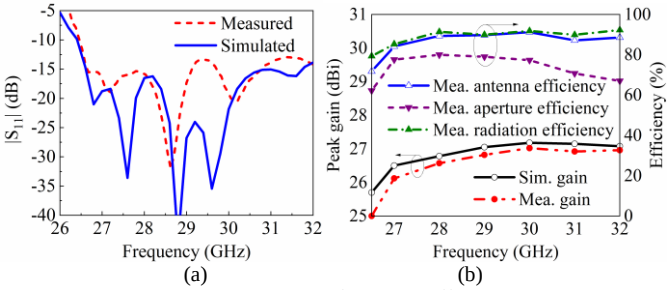

Fig. 13. (a) Simulated and measured reflection coefficient; (b) Simulated and measured peak gain and antenna efficiency.

7(a). After the phase imbalance mitigation (shown in Fig. 7(b)), the XPD is further improved by more than 3 dB, and GLL is also improved when the operating frequency is higher than 27 GHz. In all, using the proposed Type III sub-array, the FSLL and GLL are suppressed to below -26.3 dB and -27.6 dB, while the XPD is enhanced to be over 30 dB over the entire operating band.

C. Feed Network

To support the 4 × 4 sub-arrays, a 1-to-16 power divider is designed based on 1-to-2 equal power dividers with H-plane single-ridges in M3. Fig. 10 shows the whole feed network. A standard WR-28 waveguide at the center of the feed network is employed as the input port. A transition power divider is used to match the input WR-28 hollow waveguide with the output single-ridge waveguide. It should be noted that the WR-28 waveguide is rotated by 45° to be parallel with the radiation slots, which facilities the measurement. The design details of the feed network have been reported in our previous work [22]. Fig. 11 shows the simulated S-parameters of the feed network. It should be noted that the output ports are set before the ridge steps in this simulation, as they are already included in the sub-array, together with the waveguide steps (as shown in Fig. 2). The reflection coefficient is lower than -25 dB, and the output ports exhibit good amplitude and phase responses.

III. EXPERIMENTAL RESULTS

The three metallic layers (M1, M2 and M3) are fabricated using aluminum by milling. Screws are used to assemble the prototype. The photographs of the fabricated metallic layers are shown in Fig. 12(a). The overall size of the antenna is 72 mm × 72 mm × 10 mm. The radiation performance is measured using a compact-range antenna test system from MVG. The test environment is shown in

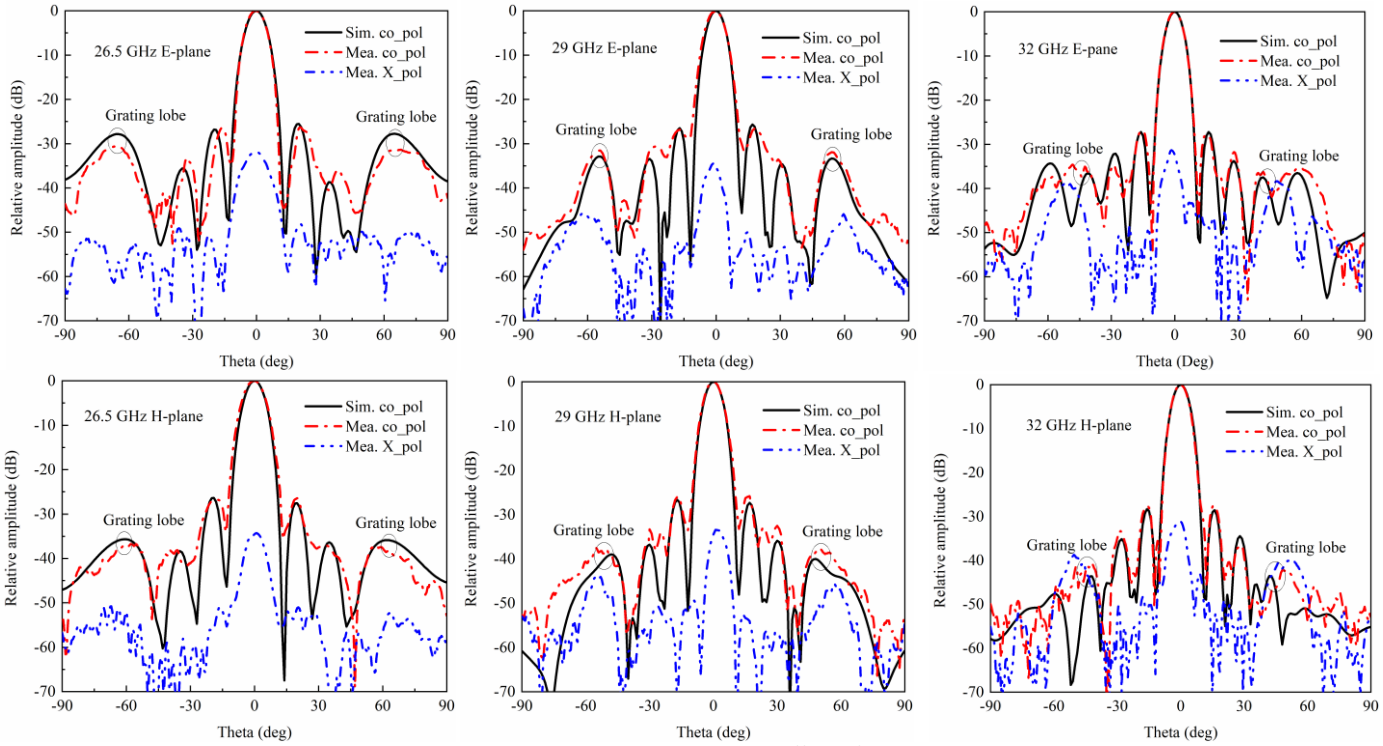

Fig. 14. Simulated and measured radiation patterns in the intended E-plane and H-plane at different frequencies.

TABLE I
PERFORMANCE COMPARISONS BETWEEN THE PROPOSED AND OTHER PUBLISHED WORKS

Ref.	Antenna type	Center frequency (GHz)/ FBW	SLL (dB)	XPD (dB)	Fabrication process	XPD suppression and method	GLL suppression and method
[22]	CTS+ separated 45° polarizer	78.5/>25%	-25.5	>32	milling	Yes, with separated polarizer	--
[23]	45°-tilted radiation slots	61.5/13.8%	-26.5	>40.5	diffusion bonding	Yes, increasing the thickness of radiation slots	Yes, additional layer of exciting slot
[24]	45°-tilted radiation slots	78.5/20.4%	-26.2	>30	diffusion bonding	Yes, with additional layer of narrow-slot pairs	Yes, additional layer of exciting slot
[26]	10°-tilted radiation slots	60/17.6%	-15	>30	die-sink electric discharge machining	--	--
This work	45°-tilted radiation slots	29.25/18.8%	-26.2	>31.3	milling	Yes, only modifying the back cavity	Yes, only modifying the back cavity

Fig. 12(b).

A. Reflection Coefficient, Peak Gain and Efficiency

Fig. 13(a) shows the simulated and measured reflection coefficients of the proposed array antenna. The measured result is obtained by using Agilent E8361C network analyzer. It is slightly higher than the simulated one, but still a good agreement is achieved. Within the frequency band of 26.5 - 32 GHz (fractional bandwidth of 18.8%), the measured reflection coefficient is lower than -10.2 dB.

The simulated and measured peak gain and antenna efficiency are plotted in Fig. 13(b). Within the operating band of 26.5 - 32 GHz, the measured peak gain varies between 25 dBi and 27 dBi, whereas the simulated one is in the range of 25.7 - 27.2 dBi. Based on the measured gain and simulated directivity, the measured radiation efficiency (excluding reflection loss) is better than 79.3% across the same frequency band. This corresponds to a measured antenna efficiency of better than 71.7%. After considering the antenna efficiency, the measured aperture efficiency is higher than 62.2%.

B. Radiation Patterns

The simulated and measured normalized radiation patterns in the intended E- and H-planes at the frequencies of 26.5 GHz, 29 GHz and 32 GHz are plotted in Fig. 14. A good agreement is achieved between the simulation and measurement. The small difference in the sidelobe distribution is mainly caused by the measured error and the imperfection in the fabrication and assembly. Over the entire operating band, the 3-dB beamwidths are larger than 7.2° in both intended E- and H-planes. The measured FSLLs at different frequencies are lower than -26.2 dB and the GLLs are suppressed to below -30.5 dB, as predicted in Fig. 9. Compared with FSLLs (about -13 dB) in the principal E- and H-planes, the first sidelobes in the intended E- and H-planes are further reduced by more than 13.2 dB. The measured cross-polarization patterns are also shown in Fig. 14. The measured XPD is more than 31.3 dB in all planes within the operating band. The measured FSLL, GLL and XPD validates the effectiveness of the design method.

C. Comparison

The comparison of this work with other 45° linearly polarized or radiation slot tilted antennas is shown in Table I. All the compared

antennas are based on hollow waveguide. Among them, the antennas in [22-24] are 45° linearly polarized. The improvement of XPD and GLL in these works was made either by using separated polarizer or additional circuit structures. This increases the number of antenna layers, which makes the antenna more complex. In [26], the antenna achieved a SLL of -15 dB, hence the radiation slots only need a rotation of 10°. In this case, the XPD remains more than 30 dB and grating lobe does not appear in the planes of φ = -10° (E-plane) and φ = 80° (H-plane). However, the deterioration of XPD and GLL occurred as the rotation angle of radiation slot increases. The 45° linearly polarized array antenna reported in this work achieved enhanced XPD and GLL suppression without additional circuit layers or separated polarizer, while keeping a good FSLL and competitive radiation performance.

IV. Conclusions

In this communication, we demonstrated a high-performance Ka-band corporate-fed 45° linearly polarized array antenna only using three metallic layers: the radiation slot layer, cavity-backed layer and feed network layer. Without any additional structure, the XPD and GLL were improved by re-designing the back cavity of the 2×2-slot sub-array, while maintaining low FSLL. A prototype was designed, fabricated and measured. Good agreement between the measurement of the prototype and simulation has been achieved. Experimental results show that the SLL is less than -26.2 dB and the XPD is more than 31.3 dB over the frequency range of 26.5 – 32 GHz. The peak gain and antenna efficiency are higher than 25 dBi and 71.7% over the same frequency band. The high performance and low profile make this antenna design being a good candidate for high-data rate mmW point-to-point communication applications.

References

[1] W. Hong et al., "Multibeam antenna technologies for 5G wireless communications," *IEEE Trans. Antennas Propag.*, vol. 65, no. 12, pp. 6231-6249, Dec. 2017.

[2] H. Ullah and F. A. Tahir, "A high gain and wideband narrow-beam antenna for 5G millimeter-wave applications," *IEEE Access*, vol. 8, pp. 29430-29434, 2020.

[3] B. Yang, Z. Yu, J. Lan, R. Zhang, J. Zhou and W. Hong, "Digital beamforming-based massive MIMO transceiver for 5G millimeter-wave communications," *IEEE Trans. Microw. Theory Tech.*, vol. 66, no. 7, pp. 3403-3418, Jul. 2018.

[4] S. Chen and A. Zhao, "LTCC based dual-polarized magneto-electric dipole antenna for 5G millimeter wave application," in *13th European Conference on Antennas and Propagation* (EuCAP), Krakow, Poland, 2019, pp. 1-4.

[5] C. Ding and K. Luk, "Wideband omnidirectional circularly polarized antenna for millimeter-wave applications using printed artificial anisotropic polarizer," in *IEEE International Symposium on Antennas and Propagation and USNC-URSI Radio Science Meeting*, Atlanta, GA, USA, 2019, pp. 1103-1104.

[6] Final Acts—World Radio communication Conference (WRC-15), *Int. Telecommun. Union-Radiocom Sector (ITU-R)*, Geneva, Switzerland, Nov. 2015

[7] 5G Americas. (2017, April). 5G Americas white paper on 5G spectrum recommendations. [Online]. Available: https://www.5gamericas.org

[8] C. Mao, M. Khalily, P. Xiao, T. W. C. Brown and S. Gao, "Planar sub-millimeter-wave array antenna with enhanced gain and reduced sidelobes for 5G broadcast applications," *IEEE Trans. Antennas Propag.*, vol. 67, no. 1, pp. 160-168, Jan. 2019.

[9] S. Zhu, H. Liu, Z. Chen and P. Wen, "A compact gain-enhanced vivaldi antenna array with suppressed mutual coupling for 5G mmWave application," *IEEE Antennas Wireless Propag. Lett.*, vol. 17, no. 5, pp. 776-779, May 2018.

[10] D. J. Bisharat, S. Liao and Q. Xue, "High gain and low cost differentially fed circularly polarized planar aperture antenna for broadband millimeter-wave applications," *IEEE Trans. Antennas Propag.*, vol. 64, no. 1, pp. 33-42, Jan. 2016

[11] M. Khalily, R. Tafazolli, P. Xiao and A. A. Kishk, "Broadband mm-wave microstrip array antenna with improved radiation characteristics for different 5G applications," *IEEE Trans. Antennas Propag.*, vol. 66, no. 9, pp. 4641-4647, Sept. 2018.

[12] B. Zhang and Y. P. Zhang, "Grid array antennas with sub-arrays and multiple feeds for 60-GHz radios," *IEEE Trans. Antennas Propag.*, vol. 60, no. 5, pp. 2270–2275, May 2012.

[13] J. Park, S. Park, W. Yang and D. G. Kam, "Folded aperture coupled patch antenna fabricated on FPC with vertically polarised end-fire radiation for fifth-generation millimeter-wave massive MIMO systems," *IET Microw., Antennas Propag.*, vol. 13, no. 10, pp. 1660-1663, Aug. 2019.

[14] D. Guan, Z. Qian, Y. Zhang and J. Jin, "High-gain SIW cavity-backed array antenna with wideband and low sidelobe characteristics," IEEE Antennas Wireless Propag. Lett., vol. 14, pp. 1774-1777, 2015.

[15] J. Xu, W. Hong, Z. H. Jiang and H. Zhang, "Wideband, low-profile patch array antenna with corporate stacked microstrip and substrate integrated waveguide feeding structure," *IEEE Trans. Antennas Propag.*, vol. 67, no. 2, pp. 1368-1373, Feb. 2019.

[16] T. Potelon, M. Ettorre and R. Sauleau, "Long slot array fed by a nonuniform corporate feed network in PPW technology," *IEEE Trans. Antennas Propag.*, vol. 67, no. 8, pp. 5436-5445, Aug. 2019.

[17] J. Liu, A. Vosoogh, A. U. Zaman and J. Yang, "A slot array antenna with single-layered corporate-feed based on ridge gap waveguide in the 60 GHz band," *IEEE Trans. Antennas Propag.*, vol. 67, no. 3, pp. 1650-1658, Mar. 2019.

[18] H. A. Diawuo, S. J. Lee, and Y. B. Jung, "Sidelobe-level reduction of a linear array using two amplitude tapering techniques," *IET Microw. Antennas Propag.*, vol. 11, no. 10, pp. 1432–1437, Aug. 2017.

[19] M. N. Ranjani and B. Sivakumar, "Design & analysis of rectangular microstrip patch antenna linear array using binomial distribution," in *Proc. 3rd Int. Conf. Electr., Electron., Comput. Eng. Their Appl.*, Apr. 2016, pp. 12–17.

[20] L. Qin, Y. Lu, Q. You, Y. Wang, J. Huang and P. Gardner, "Millimeter-wave slotted waveguide array with unequal beamwidths and low sidelobe levels for vehicle radars and communications," *IEEE Trans. Veh. Technol.*, vol. 67, no. 11, pp. 10574-10582, Nov. 2018.

[21] J. Hirokawa and M. Ando, "45° linearly polarized post wall waveguide-fed parallel plate slot arrays," *IEE Proc., Microw. Antennas Propag.*, vol. 147, pp. 515–519, Dec. 2000.

[22] Y. You et al., "High-performance E-band continuous transverse stub array antenna with a 45° linear polarizer," *IEEE Antennas Wireless Propag. Lett.*, vol. 18, no. 10, pp. 2189-2193, Oct. 2019.

[23] T. Tomura, Y. Miura, M. Zhang, J. Hirokawa and M. Ando, "A 45° linearly polarized hollow-waveguide corporate-feed slot array antenna in the 60-GHz band," *IEEE Trans. Antennas Propag.*, vol. 60, no. 8, pp. 3640-3646, Aug. 2012.

[24] T. Tomura, J. Hirokawa, T. Hirano and M. Ando, "A 45° linearly polarized hollow-waveguide 16×16-slot array antenna covering 71–86 GHz band," *IEEE Trans. Antennas Propag.*, vol. 62, no. 10, pp. 5061-5067, Oct. 2014.

[25] E. Garcia-Marin, J. L. Masa-Campos and P. Sanchez-Olivares, "Diffusion bonding manufacturing of high gain W-band antennas for 5G applications," *IEEE Commun. Mag.*, vol. 56, no. 7, pp. 21-27, Jul. 2018.

[26] A. Vosoogh, P. Kildal and V. Vassilev, "Wideband and high-gain corporate-fed gap waveguide slot array antenna with ETSI class II radiation pattern in V-Band," *IEEE Trans. Antennas Propag.*, vol. 65, no. 4, pp. 1823-1831, Apr. 2017.

[27] P. Liu, J. Liu, W. Hu and X. Chen, "Hollow waveguide 32 × 32-slot array antenna covering 71–86 GHz band by the technology of a polyetherimide fabrication," *IEEE Antennas Wireless Propag. Lett.*, vol. 17, no. 9, pp. 1635-1638, Sep. 2018.